Efficacy of platelet-inspired hemostatic nanoparticles on bleeding in Von Willebrand disease murine models

Stéphanie Roullet, Norman Luc, Julie Rayes, Jean Solarz, Dante Disharoon, Andrew Ditto, Emily Gahagan, Christa Pawlowski, Thibaud Sefiane, Frédéric Adam, et al.

Efficacy of platelet-inspired hemostatic nanoparticles on bleeding in Von Willebrand disease murine models

Stéphanie Roullet[1], Norman Luc[2], Julie Rayes[3], Jean Solarz[1], Dante Disharoon[2], Andrew Ditto[4], Emily Gahagan[4], Christa Pawlowski[4], Thibaud Sefiane[1], Frédéric Adam[1], Caterina Casari[1], Olivier D. Christophe[1], Michael Bruckman[4], Peter J. Lenting[1], Anirban Sen Gupta[2*], Cécile V. Denis[1*]

[1] Université Paris-Saclay, INSERM, Hémostase inflammation thrombose HITH U1176, 94276, Le Kremlin-Bicêtre, France
[2] Department of Biomedical Engineering, Case Western Reserve University, Cleveland, Ohio USA
[3] Institute of Cardiovascular Sciences, College of Medical and Dental Sciences, University of Birmingham, Birmingham, UK
[4] Haima Therapeutics LLC, Cleveland, Ohio USA

*: Co-corresponding authors

Corresponding author
Cécile V. Denis
Inserm U1176
80 rue du General Leclerc
94276 Le Kremlin-Bicêtre Cedex
France
Tel: +33-1-49-59-56-05
Email: cecile.denis@inserm.fr

Co-corresponding author
Anirban Sen Gupta
Case Western Reserve University
Department of Biomedical Engineering
10900 Euclid Ave., Cleveland, OH 44106
USA
Tel: +01-216-368-4564
axs262@case.edu

Abstract: 247 words
Text: 3955
Figures: 5
References: 31

Running title: Synthetic platelets efficacy in VWD murine models
Scientific category: Thrombosis and Haemostasis

Data sharing statement: Data are available upon reasonable request to the corresponding author

Key points

- Synthetic platelet nanoparticles improve thrombus formation on collagen using blood from Von Willebrand disease murine models
- Treatment with synthetic platelet nanoparticles reduces blood loss in murine models of Von Willebrand disease

Abstract

The lack of innovation in Von Willebrand disease (VWD) originates from many factors including the complexity and heterogeneity of the disease but also from a lack of recognition of the impact of the bleeding symptoms experienced by VWD patients. Recently, a few research initiatives aiming to move past replacement therapies using plasma-derived or recombinant Von Willebrand factor (VWF) concentrates have started to emerge. Here we report an original approach using synthetic platelet (SP) nanoparticles for treatment of VWD type 2B (VWD-2B) and severe VWD (type 3 VWD). SP are liposomal nanoparticles decorated with peptides enabling them to concomitantly bind to collagen, VWF and activated platelets. *In vitro,* using various microfluidic assays, we show the efficacy of SP to improve thrombus formation in VWF-deficient condition (with human platelets) or using blood from VWD-2B mice and VWF-deficient mice (VWF-KO, i.e., type 3 VWD). *In vivo*, using a tail clip assay, SP treatment reduced blood loss by 35% in VWD-2B mice and 68% in VWF-KO mice. Additional studies using nanoparticles decorated with various combinations of peptides demonstrated that the collagen binding peptide, although not sufficient by itself, was absolutely crucial for SP efficacy in VWD-2B while all three peptides appeared necessary for VWF-KO mice. Clot imaging by immunofluorescence and scanning electron microscopy revealed that SP treatment of VWF-KO mice led to a strong clot, similar to those obtained in wild-type mice. Altogether, our results show that SP could represent an attractive therapeutic alternative for VWD, especially considering their long half-life and stability.

Introduction

Treatment of Von Willebrand disease (VWD) has remained basically unchanged for the past 30 years.[1] It rests on 3 pillars: antifibrinolytics, desmopressin, and Von Willebrand factor (VWF) concentrates. However, these different approaches do not consider the heterogeneity of VWD and so far, no type or subtype-specific treatment option has been developed.

In this regard, VWD-type 2B (VWD-2B) could represent an attractive target due to its very specific nature. Indeed, VWD-2B is characterized by «gain-of-function» mutations in the VWF A1 domain, which increase VWF binding to its platelet receptor, glycoprotein (GP) Ibα. Consequently, it is the only VWD subtype associated with a platelet phenotype including the presence of circulating platelet aggregates, giant platelets, a fluctuating thrombocytopenia, and a platelet function defect.[2-4] These distinctive features raise the question of whether correcting the platelet defect could improve hemostasis in VWD-2B. Thrombocytopenia can be addressed with platelet transfusions[5] or even with thrombopoietin receptor agonists[6,7] but these approaches do not solve the thrombocytopathy since the mutant VWF will still bind spontaneously to platelet GPIbα. Strategies that can bypass the VWF-GPIbα axis while supporting platelet adhesion and aggregation may offer new possibilities to treat VWD-2B. In this regard, platelet-inspired synthetic hemostatic nanoparticles represent a very attractive alternative. These 'synthetic platelet' (SP) nanoparticles are made of a phospholipid-based liposomal template that is surface-decorated with three different peptides: a fibrinogen mimetic peptide (FMP) that can bind to the active form of platelet integrin $\alpha_{IIb}\beta_3$, a collagen-binding peptide (CBP) that can bind to exposed subendothelial fibrillar collagen, and a VWF-binding peptide (VBP), derived from the C2 domain of Factor VIII that can bind to the D'-D3 domain of VWF.[8-10] SP have been shown to collaborate with residual platelets to restore hemostatic efficacy in tail-clip model in severely thrombocytopenic mice.[11-13] Their hemostatic efficacy was also demonstrated in several animal models of traumatic injury, including a murine model of hepatic laceration,[14] a porcine model of traumatic arterial hemorrhage[15] and a rodent model of traumatic liver resection injury.[12] Due to their promising hemostatic performance efficiency in these models and their unique mode of action towards VWF, *i.e.* binding to the D'-D3 region and not to the A1-domain like platelets, we hypothesized that SP could be used to improve hemostasis in VWD-2B. Furthermore, since SP maintains the ability to bind to collagen irrespective of VWF presence[8] and still co-aggregate with active platelets to reduce bleeding, we postulated that they might also provide hemostatic support in a

situation where native platelet adhesion to VWF is lacking due to the absence of VWF. Therefore, we also tested the hemostatic capability of SP in a VWF-knockout (KO) murine model.

Methods

Additional description of the experimental procedures can be found in the Supplementary Material (available on the *Blood* website).

Animals and ethics statement

VWD-2B mice harboring the p.V1316M mutation in murine VWF and VWF-deficient mice (VWF-KO) have been described previously.[16,17] Male and female mice were used throughout the study (8-24 weeks old). This project was approved by the ethical committee CEEA26 (number APAFIS#27290-2020091714275854 v1).

Particle Manufacturing Methods

VBP and CBP were conjugated to DSPE-PEG_{2K}-Mal via thiol-maleimide coupling to form DSPE-PEG_{2K}-VBP and DSPE-PEG_{2K}-CBP and FMP was conjugated to DSPE-PEG_{2K}-azide via copper-catalyzed alkyne-azide cycloaddition (CuCAAC) or 'click chemistry' to form DSPE-PEG_{2K}-FMP. All lipid-peptide conjugates were purified by dialysis and characterized by MALDI-TOF mass spectrometry. For manufacturing liposome-based SP nanoparticles surface-decorated with all three peptides, DSPE-PEG-VBP and DSPE-PEG-CBP were combined at 1 mol% each with DSPE-PEG-FMP (15 mol%), DSPC (40 mol%), cholesterol (40 mol%), DSPE-$mPEG_{1K}$ (2 mol%), and DHPE-RhB (1 mol%) in 1:1 chloroform:methanol, subjected to solvent evaporation under reduced pressure to form thin lipid films, rehydrated with 0.9% NaCl, then subjected to 10 freeze-thaw cycles using alternating exposure to liquid nitrogen and 60°C water bath, and finally extruded five times through a 200 nm pore size polycarbonate filter (thin film rehydration and extrusion method) (Fig. 1A).[18] For nanoparticles with two, one, or no peptides, the specific lipid-peptide conjugates were replaced with an equivalent mol% of DSPE-mPEG2000, and subjected to the same process of liposomal nanoparticle fabrication as described above. Prior to use, nanoparticle size was characterized by dynamic light scattering (Fig. 1B) and cryo-transmission electron microscopy (Fig. 1C).

BioFlux microfluidic assay to study effect of SP on human platelets in absence of VWF

Human platelet suspensions in buffer, containing 200,000 platelets per µL (Plt-200k), 50,000 platelets per µL (Plt-50K) or 20,000 platelets per µL (Plt-20k) were perfused on collagen-coated channels at 60 dyn/cm^2 for 10 minutes and the green fluorescence (calcein) for surface-adhered and aggregated platelets was imaged in real time. Next, rhodamine-B labeled (red fluorescence) control nanoparticles (CP) or SP nanoparticles at a particle:platelet ratio of 1000:1 were added to Plt-50K and Plt-20K conditions, to evaluate the ability of CP *vs* SP in rescuing platelet recruitment on the collagen-coated surface.

Total thrombus formation analysis system (T-TAS®) perfusions

The T-TAS® Plus (Zacros Fujimori Kogyo, Tokyo, Japan) is an automated microchip-based flow chamber system developed for assessment of platelet thrombus formation under flow conditions.[19-21] Murine blood was collected under general anesthesia (isoflurane) by retro-orbital puncture within a non-heparinized glass capillary, in one-tenth volume trisodium citrate (13.8 mM final concentration). Blood was half-diluted in citrate solution (3.2% trisodium citrate solution/ 0.9% NaCl at the ratio of 1:9) and complemented with undecorated (control) nanoparticles or SP at a ratio of 50 particles per platelet. T-TAS® Plus perfusions were performed on AR-chips coated with collagen and tissue factor at a shear rate of 600 s^{-1} for up to 30 min. Area under the curve (AUC), representative of the increase in pressure which relates to thrombus formation, was calculated or extrapolated at 30 min.

Parallel plate flow chamber

Murine blood half-diluted in Tyrode's buffer was labeled with rhodamine 6G and complemented with control nanoparticles (CP) or SP at a ratio of 50 particles per platelet. Thrombus formation was evaluated after perfusion assay on a fibrillar collagen matrix under arterial shear conditions (shear rate of 1500 s^{-1}).[22]

Tail-clip bleeding assay

After general anesthesia with ketamine and xylazine, mice received different formulations of particles via intravenous injection (2 mg/kg, in a final volume of 100 µL NaCl 0.9%, leading to a platelet: particle ratio between 1:5 to 1:10). Ten minutes later, 3 mm of the distal tip of the tail was amputated. Blood collection and blood loss measurement were performed as

previously described.[23] Of note, bleeding was assessed over 30 min for VWD-2B and 20 min for VWF-KO mice.

Immunofluorescence imaging of amputated tails

At the end of the tail-clip bleeding assay, 1 cm of the distal tip of tails from VWF wild-type (WT) mice or VWF-KO mice injected with SP was amputated and fixed in 4% paraformaldehyde (PFA) for 24 h. Sections were stained for platelets using an anti-mouse CD41 antibody and for fibrin. Analysis was done in a selected region of interest which was defined inside the vessel. Sections were imaged using epifluorescent microscopy and analyzed using ImageJ software.

Scanning electron microscopy observation of clot morphology after tail vein transection

Untreated VWF-KO mice or VWF-KO mice injected with SP underwent a tail vein transection procedure as previously described.[24] After 10 min, the tail was immersed in 4% PFA/1% glutaraldehyde and cut. The sample was then immediately immersed in 10 ml 4% PFA/1% glutaraldehyde and fixed overnight at 4°C. Then, a 1 cm tail section was cut, centered on injury. A "Nanosuit" was used to protect the samples from electron beam and hard drying [25] The tails were dipped three times during one minute in the nanosuit and then pre-irradiated by a sputtering device without the metal emitter. Finally, silver metallization (setting: 10 nm of silver: 120 seconds at 5 cm and 30 mA) of the complete tail section was performed, and the samples were observed with scanning electron microscopy at different magnifications.

Statistical analysis

Data are presented as mean±standard deviation (SD) unless indicated otherwise. Mann-Whitney test was performed for two-groups comparison. One-way analysis of variance (ANOVA) followed by Tukey's multiple comparison test was performed when comparing multiple groups. P <0.05 was considered statistically significant. Statistical analysis was performed using GraphPad Prism 7 software (La Jolla, CA, USA).

Results

SP enhances platelet surface-coverage in BioFlux microfluidics in VWF-deficient condition

Fig. 1D shows representative fluorescence images of platelet surface-coverage in Plt-200k *vs* Plt-20k *vs* 'Plt-20k + CP' *vs* 'Plt-20k + SP' conditions on collagen-coated BioFlux microfluidic channels in the absence of any plasma VWF. As evident from the images, the surface coverage was drastically reduced in Plt-20K condition compared to Plt-200K condition. Adding CP in Plt-20K condition did not rescue or improve platelet surface-coverage. In contrast, adding SP in Plt-20K condition substantially improved platelet surface-coverage, and a high co-localization of red SP nanoparticles with green platelets was observed (appearing yellow in the merged image), suggesting that SP nanoparticles were able to rapidly bind to the exposed collagen even in the absence of VWF and enable concomitant binding of active platelets onto them to render enhanced recruitment and coverage of platelets on the surface. Fig. 1E shows quantitative analysis of the results from these studies (n = 5 per condition), confirming that surface-coverage of platelets on collagen-coated microchannels is significantly reduced (P<0.0001) in Plt-20K condition (1.2±0.8%) compared to Plt-200K condition (14.5±3.2%), and addition of SP significantly rescued (7.0±2.2%, P=0.0014) this surface-coverage compared to addition of CP (1.4±0.9%). Surface-averaged platelet fluorescence intensity (green fluorescence, arbitrary units) from the same conditions, normalized to Plt-200K condition, are shown in Fig. S1. Supplementary movies A, B, C and D show representative microfluidic imaging of Plt-200K, Plt-20K, Plt-20K + CP and Plt-20K + SP conditions. Additionally, Fig. S2 shows representative fluorescence images and quantitative analysis data for SP treatment of Plt-50K condition, once again indicating the ability of SP to rescue platelet coverage on collagen-coated microfluidic surface. Altogether, these results indicate that SP nanoparticles can potentially render improved hemostatic responses in VWF-deficient and platelet-depleted conditions, as long as the concomitant collagen-binding (via CBP) and integrin $\alpha_{IIb}\beta_3$-binding (via FMP) properties of SP are able to enhance the recruitment of active platelets on collagen-exposing surface.

Ex-vivo addition of SP to VWD blood improves T-TAS® perfusions' parameters

In the T-TAS® perfusion system, the AUC is an integrated parameter, representative of the pressure generated by platelet adhesion and thrombus formation inside a collagen- and tissue factor-coated chip. By analyzing changes in pressure as a function of time, Fig. 2A left panel clearly shows that SP addition to murine VWD-2B blood led to a significant increase in AUC (1308 with a 95%CI 1278-1329) compared to untreated VWD-2B blood (710, 95%CI 687-734, *P*<0.0001) or to undecorated/CP-supplemented blood (733, 95%CI 717-748, *P*<0.0001). For murine VWF-KO blood, we also measured significantly increased AUC when blood was supplemented with SP (988, 95%CI 954-1022) compared to untreated blood (422, 95%CI 407-436, *P*<0.0001) or to CP-treated blood (558, 95%CI 541-575, *P*<0.0001) (Fig. 2A, right panel). For SP-treated VWD-2B or SP-treated VWF-KO blood, the AUC remained lower than for wild-type blood (1916, 95%CI 1900-1933), indicating that thrombus formation was not completely rescued.

Altogether, the T-TAS® perfusion assays show a significant improvement of platelet adhesion when SP were added to VWD blood.

Ex-vivo addition of SP to VWD blood significantly improved thrombus formation in a parallel plate flow chamber

To build on the encouraging results obtained with the T-TAS® system, additional blood perfusion studies were performed using a more "classical" collagen-coated parallel plate flow chamber. Addition of SP to VWD-2B blood significantly increased thrombus formation compared to both untreated blood or blood supplemented with CP (174±59 *vs* 58±9, *P*=0.016 and 174±34 *vs* 55±2, *P*=0.015, respectively) (Fig. 2B, upper panels) as measured by the mean fluorescent intensity, a surrogate marker for thrombus size (Fig. 2C, left panel).

Addition of SP to VWF-KO blood also led to a strong increase in thrombus formation compared to untreated blood (523±213 *vs* 28±14, *P*=0.002) and blood supplemented with CP (523±213 *vs* 31±2, *P*=0.003), (Fig. 2B, bottom panels and Fig. 2C, left panel). Interestingly thrombi formed in VWF-KO blood supplemented with SP appeared bigger than those formed in VWD-2B supplemented with SP.

In terms of percentage platelet coverage, SP addition to VWF-KO blood led to an increase in platelet adhesion (Fig. 2C, right panel) with 20±2% covered area compared to 5.2±1.9% with untreated blood and 5.3±2% with CP. The results are less clear with VWD-2B blood where in terms of percentage covered area, an increase was seen only in the presence of CP (24±3.4%)

compared to untreated blood (13.4±3.7%) or to SP-supplemented blood (13.4±0.2%). However, despite this increased surface coverage seen with control particles, no thrombus formation was observed.

Compared to wild-type conditions, only thrombus size obtained in SP-treated VWF-KO blood was normalized. All other parameters remained below wild-type read-outs.

Co-localization of platelets with SP can clearly been seen when both entities were labeled with distinct fluorochromes in thrombi formed using SP-treated VWF-KO blood (Fig. S3).

SP significantly reduced bleeding in VWD mice

We next assessed the bleeding phenotype of VWD-2B and VWF-KO mice treated with SP. As expected, untreated VWD-2B mice lost large amounts of blood compared to WT mice (938±161 *vs* 18±17 µL, *P*<0.0001; Fig. 3A). Treatment with CP did not improve hemostasis in these mice (966±192 *vs* 938±161 µL, *P*=0.98). In contrast, addition of SP significantly reduced blood loss by an average of 35% (631±199 *vs* 966±192 µL with control particles, P<0.001 and 631±199 *vs* 938±161 µL without treatment, *P*=0.001). Nevertheless, complete correction was not obtained (631±199 *vs* 18±17 µL in WT mice, *P*<0.0001) (Fig. 3A). Of note, SP did not affect the multimeric profile of VWD-2B mice (Fig. S4).

For VWF-KO mice, untreated mice as well as CP treated-mice bled profusely compared to WT mice (561±207 µL and 539±194 µL *vs* 19±17 µL) (Fig.3B). SP treatment of VWF-KO mice demonstrated an important efficacy in reducing bleeding (183±167 µL *vs* 561±207 µL in untreated mice, *P*=0.01). Strikingly, blood loss after SP treatment was no longer statistically different than blood loss in WT mice (183±167 µL *vs* 19±17 µL, *P*=0.15). SP thus appeared more efficient in VWF-KO mice compared to VWD-2B mice, probably due to the platelet function defect described in the latter model.

Mechanisms underlying hemostatic efficacy of SP in VWD

In order to investigate whether the three different peptides were equally important in the hemostatic efficiency of SP in VWD murine models, we tested different combinations of particles harboring only one peptide or combinations of two peptides (Fig. 4).

In VWD-2B, particles decorated with any of the single peptides were not efficient in reducing blood loss (CBP: 761±287 µL, FMP: 1072±174 µL and VBP: 856±125 µL *vs* 966±192 µL with CP, *P*=0.08, 0.71 and 0.81 respectively). Second, when using particles decorated with

combinations of two peptides, only 'CBP + VBP' and 'CBP + FMP' combinations were as efficient as SP in correcting blood loss (CBP+VBP: 587±255 µL and CBP+FMP: 568±173 µL *vs* 631±199 µl with SP; *P*=0.99 and =0.97 respectively). In contrast, particles decorated with the 'VBP + FMP' combination did not show any efficacy (929±156 µL *vs* 966±192 µL with CP, *P*=0.99) (Fig. 4A).

In VWF-KO mice, similar to VWD-2B mice, particles decorated with single peptides were not efficient in reducing blood loss with even a slight increase with FMP (CBP: 636±239 µL, FMP: 859±161 µL, VBP: 618±200 µL *vs* 539±194 µL with CP, *P*=0.16, 0.0016 and 0.82 respectively). Surprisingly, the combination of CBP+FMP was less efficient in reducing blood loss than SP (530±100 µL *vs* 183±167 µL, *P*=0.0001), pointing to an unexpected effect of the VBP (Fig. 4B), likely due to the phospholipid binding capacity of this factor-VIII derived peptide. However, particles decorated with VBP only did not show any hemostatic efficacy. Complete statistical analysis is provided in Supplementary Table 1.

In conclusion, CBP appears to be the most important peptide in the SP but is not sufficient by itself to support hemostasis in VWD-2B mice while all three peptides are necessary in VWF-KO mice.

SP colocalizes with platelets and fibrin in the clot observed after tail-clip

We next sought to image the clots observed after SP treatment in the tail clip experiment. Here, we only imaged clots from the treated VWF-KO mice. SP, labeled with Rhodamine B could be seen as colocalizing with platelets and fibrin in the clots formed in VWF-KO mice after SP treatment (Fig. 5A). A large clot, occluding the vessel from side to side could clearly be seen in SP-treated VWF-KO mice. Although this experiment is mostly of a qualitative nature, our attempt to quantify these data suggested that both the area and fluorescence intensity of the platelets and fibrin signals were similar to those obtained after imaging of a clot formed in WT mice (Fig. 5B).

SP leads to substantial hemostatic clot as visible by scanning electron microscopy

To extend our observation of the SP-induced clot formation in VWF-KO mice, we collected the clot obtained after lateral tail vein transection in untreated and SP-treated mice. On the upper panels of Fig. 5C, the sectioned hair indicates the area where the cut was performed (shown by the black arrows). In the untreated VWF-KO mouse, a thin thrombus could be spotted as

covering the scar, thrombus formed of individualized red blood as visible at higher magnification. Upon SP treatment (Fig. 5C, right panels), a larger thrombus was visible, covering the entire scar section with red blood cells aggregated together in the clot.

Discussion

Platelet-mimicking nanoparticles are currently under pre-clinical development to mitigate bleeding in various hemostatic dysfunction settings spanning thrombocytopenia, coagulopathy and trauma.[11-15] However, they have not yet been tested in congenital bleeding disorders linked to platelet and VWF defects. Considering our team's current interest in developing tailored therapeutic options for different VWD types/subtypes, we hypothesized that, by circumventing the VWF-GPIbα axis, SP could represent an attractive option for VWD type 2B. *In vitro*, using a Bioflux microfluidic system, we first showed the capacity of SP to rescue human platelet recruitment in thrombocytopenic conditions and in VWF-deficient conditions, serving as a basis for testing their efficacy in our VWD-2B and VWF-KO mouse models. Next, using VWD-2B or VWF-KO murine blood, we confirmed that SP indeed significantly improved thrombus formation in perfusion assays both in a regular parallel plate perfusion chamber (Maastricht flow chamber),[26] as well as in the T-TAS® assay.

Building on these *in vitro* results, and when injected *in vivo*, SP were able to reduce bleeding in VWD-2B mice and to achieve near-complete correction of hemostasis in VWF-KO mice. These results raise a number of questions: firstly, regarding why SP are functional in VWF-KO mice since platelets are fully functional in these mice, and second, why SP are more efficient in the VWF-KO compared to VWD-2B mice? SP have been shown to collaborate with platelets[10-13] and in the absence of platelet-VWF interaction in VWF-KO mice, we can rationalize that the adhesion of SP to vascular collagen creates a new *landing platform* for native platelets to adhere to. Platelets would therefore be recruited to sites of vascular injury *via* SP, a hypothesis supported by the co-localization of SP with platelets and fibrin following tail-clip injury. As to why SP display higher efficiency in VWF-KO mice compared to VWD-2B animals, it should be emphasized that the latter model is characterized by thrombocytopenia/thrombocytopathy. Platelet counts in VWD-2B mice are reduced by 50% compared to VWF-KO.[16] Although this decrease is not very profound, the inability of these VWD-2B platelets to fully activate[27] may also explain why less coagulation will take place on their surface, limiting fibrin formation and ultimately, hampering bleeding correction.

To investigate mechanisms by which SP contributed to haemostasis in VWD mice, we tested several types of particles decorated with different peptide combinations. In VWD-2B mice, only particles decorated with combination of 'CBP + VBP' and 'CBP + FMP' proved as efficient

as SP to reduce bleeding, highlighting the pivotal role of collagen in injury site-specific particle anchoring and haemostatic action. However, the CBP alone was not efficient, suggesting that at least, another platelet-mimicking characteristic was necessary for particle efficiency. Nevertheless, restoring full haemostasis in VWD-2B remains difficult since both defects in VWF and in platelets need to be overcome.[28] New generations of platelet-inspired nanoparticles are currently under development: platelet-mimicking procoagulants nanoparticles, with a plasmin-triggered exposure of phosphatidylserine at the site of injury,[12] or the release of thrombin at the site of injury.[29] Increasing site-specific coagulation outputs with such particles might be key to improve their potential use in VWD-2B. It should also be emphasized that our VWD-2B mouse model carries the p.V1316M variant, one of the most severe VWD-2B causing mutation. Milder forms of VWD-2B may potentially be more responsive to SP treatment.

In VWF-KO mice, the result that the combination of 'CBP+FMP' was less efficient than SP to correct the haemostatic defect can appear very surprising at first glance. Indeed, VBP, the missing peptide in these dual-decorated particles, should be of no use in the absence of VWF. However, this VBP is derived from the FVIII C2 domain and binds not only to the VWF D'-D3 region but also to phospholipids.[8] It seems conceivable therefore that even in the absence of VWF, this peptide contributes to the hemostatic response by re-enforcing the interactions between SP and activated platelets. However, particles decorated with the VBP peptide alone have no hemostatic efficiency by themselves. Although theoretically, this peptide could compete with FVIII for VWF binding in the VWD-2B mice, this is unlikely to occur given that its concentration (≤500 nM) is lower than the IC50 (6 µM).[30]

Imaging of the clots in the presence of SP was carried out only in VWF-KO mice for technical reasons. Indeed, imaging clots of bleeding mice, such as was the case for VWD-2B mice, proved unsuccessful. The clots obtained in VWF-KO mice treated with SP appeared very similar to those obtained in wild-type mice as visible by fluorescent analysis. The overlap between platelets and fibrin in SP-treated mice suggests that by recruiting platelets, SP contribute not only directly to the formation of the platelet-enriched thrombus but also indirectly to the availability of platelet-exposed procoagulant phospholipids on which coagulation can occur. Scanning electron microscopy confirmed that SP led to a more compact and solid thrombus than those obtained in untreated VWF-KO mice.

So where does such an approach fit as a potential treatment for VWD? Originally, the study was intended to test a new therapeutic for VWD-2B but, although promising, the SP particle

design does not appear to be optimally efficient in this VWD subtype. However, this technology has the advantage that it can be further tailored for augmenting coagulation by incorporating additional pro-hemostatic molecules on the particle surface or in the particle core, mimicking platelet's procoagulant and secretory functions. Therefore, the present study should be seen as a first proof-of-concept that platelet-mimicking particles can be used for VWD-2B patients. For severe VWD (type 3), SP particles have proven very efficient. Due to their unique characteristics, they can thus be considered as a potential new therapeutic approach for severe VWD. Indeed, their manufacturing process and stability, *i.e.* lyophilizability, no requirement for cold storage and >6 months shelf-life, may render them very attractive compared to VWF concentrates. Furthermore, from a pharmacokinetic point of view, SP have a clear advantage over VWF concentrates. In mice, 2 hours after injection, only about 10% of VWF can still be detected.[31] In contrast, 2 hours after injection in mice, only 15% of SPs have been cleared from the circulation,[13] and recent studies with procoagulant platelet-mimicking particles have reported a half-life of 12 hours.[12] SP thus display a much longer circulatory half-life than VWF. The use of SP could also be considered in severe VWD patients who have developed allo-antibodies, precluding the use of VWF concentrates.

Altogether, there is clearly room for such a technology in a VWD setting and our results warrant further investigation of platelet-inspired nanoparticles as a novel strategy for the hemostatic management of VWD.

Acknowledgements

The work was supported by INSERM (Institut National de la Santé et de la Recherche Médicale) and by the Agence Nationale de la Recherche (ANR-21-CE14-0076-01 to CVD). JR holds a British Heart Foundation (BHF) Intermediate Fellowship (FS/IBSRF/20/25039). ASG is supported by NIH R01 HL121212.

Authorship Contributions

SR, NL, JR, JS, DD, TS, FA, CCC, ODC, PJL and CVD performed experiments and analyzed the data. AD, EG, CP, MB and ASG provided essential reagents. JR, PJL, ASG and CVD designed the study. SR, CVD and ASG wrote the manuscript. All authors contributed to the final editing of the manuscript.

Disclosure of Conflicts of Interest

AD, EG, CP and MB are employees of Haima Therapeutics LLC. ASG is co-founder and chief scientific advisor for Haima Therapeutics.

References

1. Denis CV, Susen S, Lenting PJ. von Willebrand disease: what does the future hold? *Blood.* 2021;137(17):2299-2306.
2. Casari C, Berrou E, Lebret M, et al. von Willebrand factor mutation promotes thrombocytopathy by inhibiting integrin alphaIIbbeta3. *J Clin Invest.* 2013;123(12):5071-5081.
3. Federici AB, Mannucci PM, Castaman G, et al. Clinical and molecular predictors of thrombocytopenia and risk of bleeding in patients with von Willebrand disease type 2B: a cohort study of 67 patients. *Blood.* 2009;113(3):526-534.
4. Kauskot A, Poirault-Chassac S, Adam F, et al. LIM kinase/cofilin dysregulation promotes macrothrombocytopenia in severe von Willebrand disease-type 2B. *JCI Insight.* 2016;1(16):e88643.
5. Kruse-Jarres R, Johnsen JM. How I treat type 2B von Willebrand disease. *Blood.* 2018;131(12):1292-1300.
6. Casari C, Favier R, Legendre P, et al. A thrombopoietin receptor agonist to rescue an unusual platelet transfusion-induced reaction in a p.V1316M-associated von Willebrand disease type 2B patient. *Ther Adv Hematol.* 2022;13:20406207221076812.
7. Espitia O, Ternisien C, Agard C, Boisseau P, Denis CV, Fouassier M. Use of a thrombopoietin receptor agonist in von Willebrand disease type 2B (p.V1316M) with severe thrombocytopenia and intracranial hemorrhage. *Platelets.* 2017;28(5):518-520.
8. Haji-Valizadeh H, Modery-Pawlowski CL, Sen Gupta A. A factor VIII-derived peptide enables von Willebrand factor (VWF)-binding of artificial platelet nanoconstructs without interfering with VWF-adhesion of natural platelets. *Nanoscale.* 2014;6(9):4765-4773.
9. Ravikumar M, Modery CL, Wong TL, Dzuricky M, Sen Gupta A. Mimicking adhesive functionalities of blood platelets using ligand-decorated liposomes. *Bioconjug Chem.* 2012;23(6):1266-1275.
10. Ravikumar M, Modery CL, Wong TL, Gupta AS. Peptide-decorated liposomes promote arrest and aggregation of activated platelets under flow on vascular injury relevant protein surfaces in vitro. *Biomacromolecules.* 2012;13(5):1495-1502.

11. Luc NF, Rohner N, Girish A, Didar Singh Sekhon U, Neal MD, Sen Gupta A. Bioinspired artificial platelets: past, present and future. *Platelets.* 2022;33(1):35-47.
12. Sekhon UDS, Swingle K, Girish A, et al. Platelet-mimicking procoagulant nanoparticles augment hemostasis in animal models of bleeding. *Sci Transl Med.* 2022;14(629):eabb8975.
13. Shukla M, Sekhon UD, Betapudi V, et al. In vitro characterization of SynthoPlate (synthetic platelet) technology and its in vivo evaluation in severely thrombocytopenic mice. *J Thromb Haemost.* 2017;15(2):375-387.
14. Dyer MR, Hickman D, Luc N, et al. Intravenous administration of synthetic platelets (SynthoPlate) in a mouse liver injury model of uncontrolled hemorrhage improves hemostasis. *J Trauma Acute Care Surg.* 2018;84(6):917-923.
15. Hickman DA, Pawlowski CL, Shevitz A, et al. Intravenous synthetic platelet (SynthoPlate) nanoconstructs reduce bleeding and improve 'golden hour' survival in a porcine model of traumatic arterial hemorrhage. *Sci Rep.* 2018;8(1):3118.
16. Adam F, Casari C, Prevost N, et al. A genetically-engineered von Willebrand disease type 2B mouse model displays defects in hemostasis and inflammation. *Sci Rep.* 2016;6:26306.
17. Denis C, Methia N, Frenette PS, et al. A mouse model of severe von Willebrand disease: defects in hemostasis and thrombosis. *Proc Natl Acad Sci U S A.* 1998;95(16):9524-9529.
18. Zhang H. Thin-Film Hydration Followed by Extrusion Method for Liposome Preparation. *Methods Mol Biol.* 2017;1522:17-22.
19. Hosokawa K, Ohnishi T, Fukasawa M, et al. A microchip flow-chamber system for quantitative assessment of the platelet thrombus formation process. *Microvasc Res.* 2012;83(2):154-161.
20. Hosokawa K, Ohnishi T, Kondo T, et al. A novel automated microchip flow-chamber system to quantitatively evaluate thrombus formation and antithrombotic agents under blood flow conditions. *J Thromb Haemost.* 2011;9(10):2029-2037.
21. Sueta D, Kaikita K, Okamoto N, et al. A novel quantitative assessment of whole blood thrombogenicity in patients treated with a non-vitamin K oral anticoagulant. *Int J Cardiol.* 2015;197:98-100.

22. Adam F, Kauskot A, Nurden P, et al. Platelet JNK1 is involved in secretion and thrombus formation. *Blood.* 2010;115(20):4083-4092.
23. Ferriere S, Peyron I, Christophe OD, et al. A hemophilia A mouse model for the in vivo assessment of emicizumab function. *Blood.* 2020;136(6):740-748.
24. Johansen PB, Tranholm M, Haaning J, Knudsen T. Development of a tail vein transection bleeding model in fully anaesthetized haemophilia A mice - characterization of two novel FVIII molecules. *Haemophilia.* 2016;22(4):625-631.
25. Takaku Y, Suzuki H, Kawasaki H, et al. A modified 'NanoSuit(R)' preserves wet samples in high vacuum: direct observations on cells and tissues in field-emission scanning electron microscopy. *R Soc Open Sci.* 2017;4(3):160887.
26. Provenzale I, Brouns SLN, van der Meijden PEJ, Swieringa F, Heemskerk JWM. Whole Blood Based Multiparameter Assessment of Thrombus Formation in Standard Microfluidic Devices to Proxy In Vivo Haemostasis and Thrombosis. *Micromachines (Basel).* 2019;10(11).
27. Casari C, Paul DS, Susen S, et al. Protein kinase C signaling dysfunction in von Willebrand disease (p.V1316M) type 2B platelets. *Blood Adv.* 2018;2(12):1417-1428.
28. Rayes J, Hollestelle MJ, Legendre P, et al. Mutation and ADAMTS13-dependent modulation of disease severity in a mouse model for von Willebrand disease type 2B. *Blood.* 2010;115(23):4870-4877.
29. Girish A, Jolly K, Alsaadi N, et al. Platelet-Inspired Intravenous Nanomedicine for Injury-Targeted Direct Delivery of Thrombin to Augment Hemostasis in Coagulopathies. *ACS Nano.* 2022.
30. Saenko EL, Shima M, Rajalakshmi KJ, Scandella D. A role for the C2 domain of factor VIII in binding to von Willebrand factor. *J Biol Chem.* 1994;269(15):11601-11605.
31. Lenting PJ, Westein E, Terraube V, et al. An experimental model to study the in vivo survival of von Willebrand factor. Basic aspects and application to the R1205H mutation. *J Biol Chem.* 2004;279(13):12102-12109.

Figure Legends

Figure 1. Physical and functional characterization of the synthetic platelet (SP) nanoparticles

A) Schematic of the manufacturing process for synthetic platelet (SP) nanoparticle with lipids and lipid-peptide conjugates using the thin film rehydration followed by extrusion methodology.

B) Dynamic Light Scattering (DLS) characterization and C) Cryo-transmission electron microscopy (Cryo-TEM) imaging of SP nanoparticles indicates a diameter of approximately 150-200 nm.

D-E) Representative fluorescence microscopy images and quantitative analysis of imaging data from BioFlux microfluidics studies with platelet suspensions indicate that depletion of platelets from 200,000 per µL (Plt-200K) to 20,000 per µL (Plt-20K) results in drastic reduction of platelet coverage of collagen-coated microfluidic channel surface. Treatment of Plt-20K with control nanoparticles (CP) does not rescue this while treatment of Plt-20K with SP nanoparticles significantly rescues platelet recruitment and coverage on the collagen-coated channel surface (colocalization of Rhodamine B-labeled red fluorescent SP with calcein-stained green fluorescent platelets appear yellow). The particle/platelet ratio was 1000:1. Means ± SD are represented. Statistical analysis was performed using a one-way Anova with Tukey's correction. ns: non-significant, ** $P \leq 0.01$, *** $P \leq 0.001$, **** $P \leq 0.0001$.

Figure 2. *In vitro* effect of SP nanoparticles added to VWD murine blood in perfusion assays

A) Synthetic platelets or control nanoparticles were added to VWD-2B blood (left panel) or to VWF-KO blood (right panel) at a ratio of 50 particles per platelet. Particle-supplemented blood or unsupplemented blood (untreated) was perfused over AR chips in the T-TAS® Plus system. Graphs represent changes in pressure (a measure for thrombus formation) as a function of time. The colored area represents the standard error of the mean (SEM) for each condition. Statistical analysis was performed using a one-way Anova with Tukey's correction.

B-C) Synthetic platelets or control nanoparticles were added to VWD-2B murine blood or to VWF-KO murine blood at a ratio of 50 particles per platelet. Particle-supplemented blood or unsupplemented blood (untreated) was perfused over collagen in a parallel flow chamber at 1500 s^{-1}. untreated Representative images of thrombus formation are shown in B while percentage platelet coverage, representing adhesion or mean fluorescence intensity (MFI) as

a marker of thrombus size are represented in C. Results obtained with untreated wild-type murine blood is shown for comparison. Data are presented as mean ± SD. n=3. Statistical analysis was performed using a one-way Anova with Tukey's correction. ns: not significant, * $P \leq 0.05$, ** $P \leq 0.01$, **** $P \leq 0.0001$. a.u.: arbitrary units.

Figure 3. *In vivo* effect of SP nanoparticles in VWD-2B and VWF-KO murine models

Mice were injected or not with control nanoparticles or synthetic platelet nanoparticles (2 mg/kg). Bleeding was measured for 30 min (VWD-2B) (A) or 20 min (VWF-KO) (B) after amputation of 3 mm of the tail tip. Blood was collected in warm saline and quantified using a hemoglobin calibration curve. Each dot represents an individual mouse. Data are presented as mean ± SD. Statistical analysis was performed using a one-way Anova with Dunnett's correction. ns: not significant, * $P \leq 0.05$, *** $P \leq 0.001$, **** $P \leq 0.0001$. WT: wild-type.

Figure 4. *In vivo* effect of various peptide-decorated particles in VWD-2B and VWF-KO murine models

Mice were injected with control particles, synthetic platelets nanoparticles or particles decorated with various combinations of peptides (2 mg/kg). Bleeding was measured for 30 min (VWD-2B) (A) or 20 min (VWF-KO) (B) after amputation of 3 mm of the tail tip. Blood was collected in warm saline and quantified using a hemoglobin calibration curve. Each dot represents an individual mouse. Data are presented as mean ± SD. Statistical analysis was performed using a one-way Anova with Dunnett's correction. ** $P \leq 0.01$, *** $P \leq 0.001$, **** $P \leq 0.0001$. Synthetic platelets nanoparticles (3 peptides) are represented with the even grey bar while particles decorated with dual peptides appear in diagonally-striped bars and single-decorated particles appear in horizontally-striped bars. CBP: collagen binding peptide; FMP: fibrinogen mimetic peptide; VBP: Von Willebrand factor binding peptide.

Figure 5. Imaging of the clots obtained after synthetic platelets (SP) treatment of VWF-KO mice

A) Representative images of the fluorescent staining of clots recovered after amputation of the tail tip of VWF WT mice and VWF-KO mice injected with SP (2mg/kg). Dashes represent the vessel's edges. Rhodamine-labeled SP are visible in red, fibrin/fibrinogen is visible in magenta and CD41-labeled platelets appear in green.

B) Quantification of the platelets (CD41+) and fibrin area and fluorescence intensity in WT (n=3) and VWF-KO mice injected with SP (n=3). Data are presented as mean ± SD. Statistical analysis was performed using a Mann-Whitney test.

C) Scanning electron microscopy of the clot recovered after tail vein transection in untreated VWF-KO mouse and SP-treated VWF-KO mouse. On the upper images, black arrows indicate the transection area recognizable by the hair that appear sectioned and the blue arrows point to the clot. On the bottom left image, red arrows show individualized red blood cells. On the bottom right image, blue arrow shows the clot characterized by aggregated red blood cells and red arrows show individualized red blood cells. Two mice per group were imaged and representative images are shown.

Figure 1

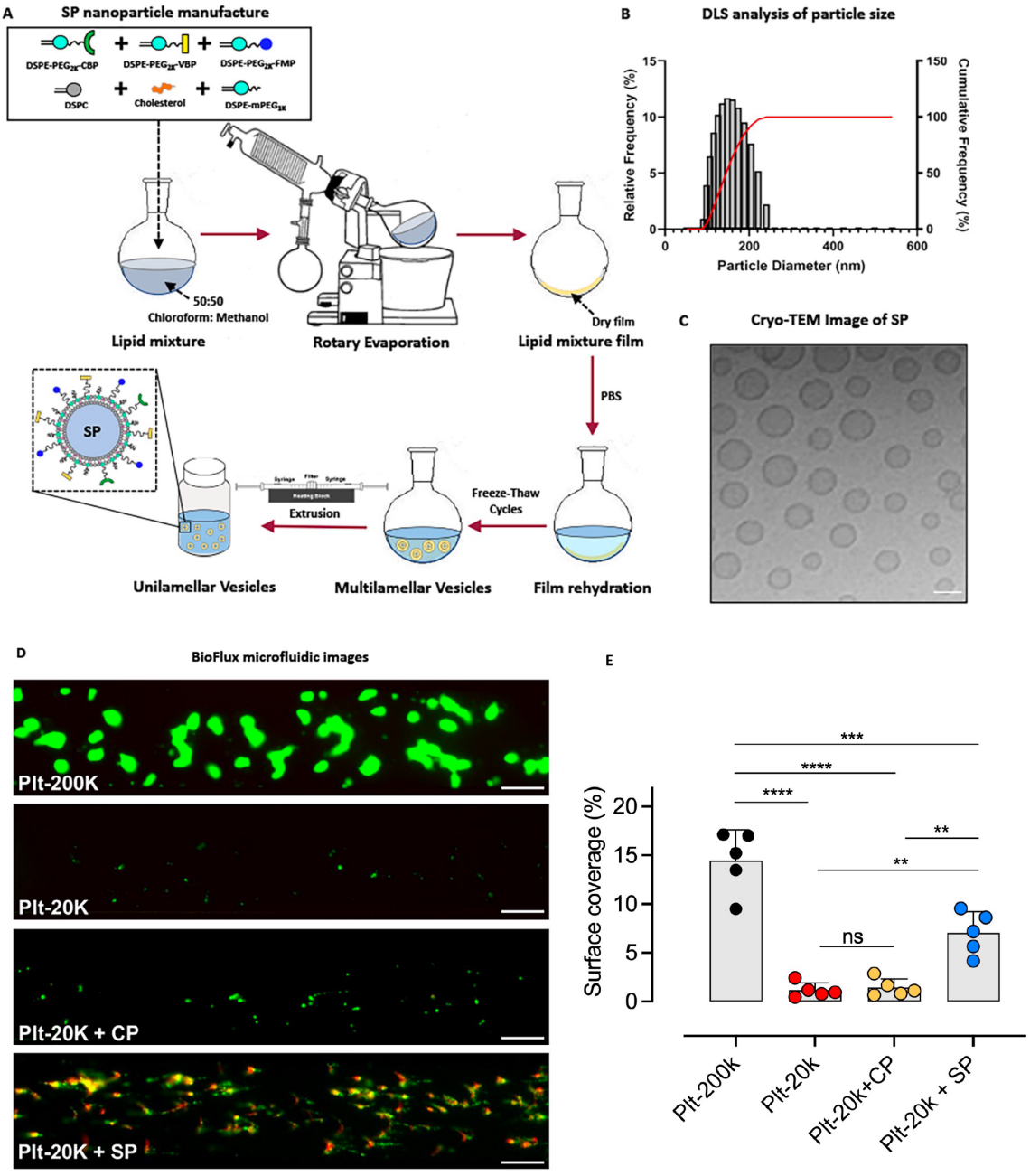
A
SP nanoparticle manufacture
DSPE-PEG2K-CBP
DSPE-PEG2K-VBP
DSPE-PEG2K-FMP
DSPC
Cholesterol
DSPE-mPEG1K
50:50
Chloroform: Methanol
Lipid mixture
Rotary Evaporation
Dry film
Lipid mixture film
PBS
SP
Extrusion
Freeze-Thaw
Cycles
Unilamellar Vesicles
Multilamellar Vesicles
Film rehydration
B
DLS analysis of particle size
Relative Frequency (%)
Cumulative Frequency (%)
Particle Diameter (nm)
C
Cryo-TEM Image of SP
D
BioFlux microfluidic images
PIt-200K
PIt-20K
PIt-20K + CP
PIt-20K + SP
E
Surface coverage (%)
***
****
****
**
**
ns
PIt-200k
PIt-20k
PIt-20k+CP
PIt-20k + SP

Figure 2

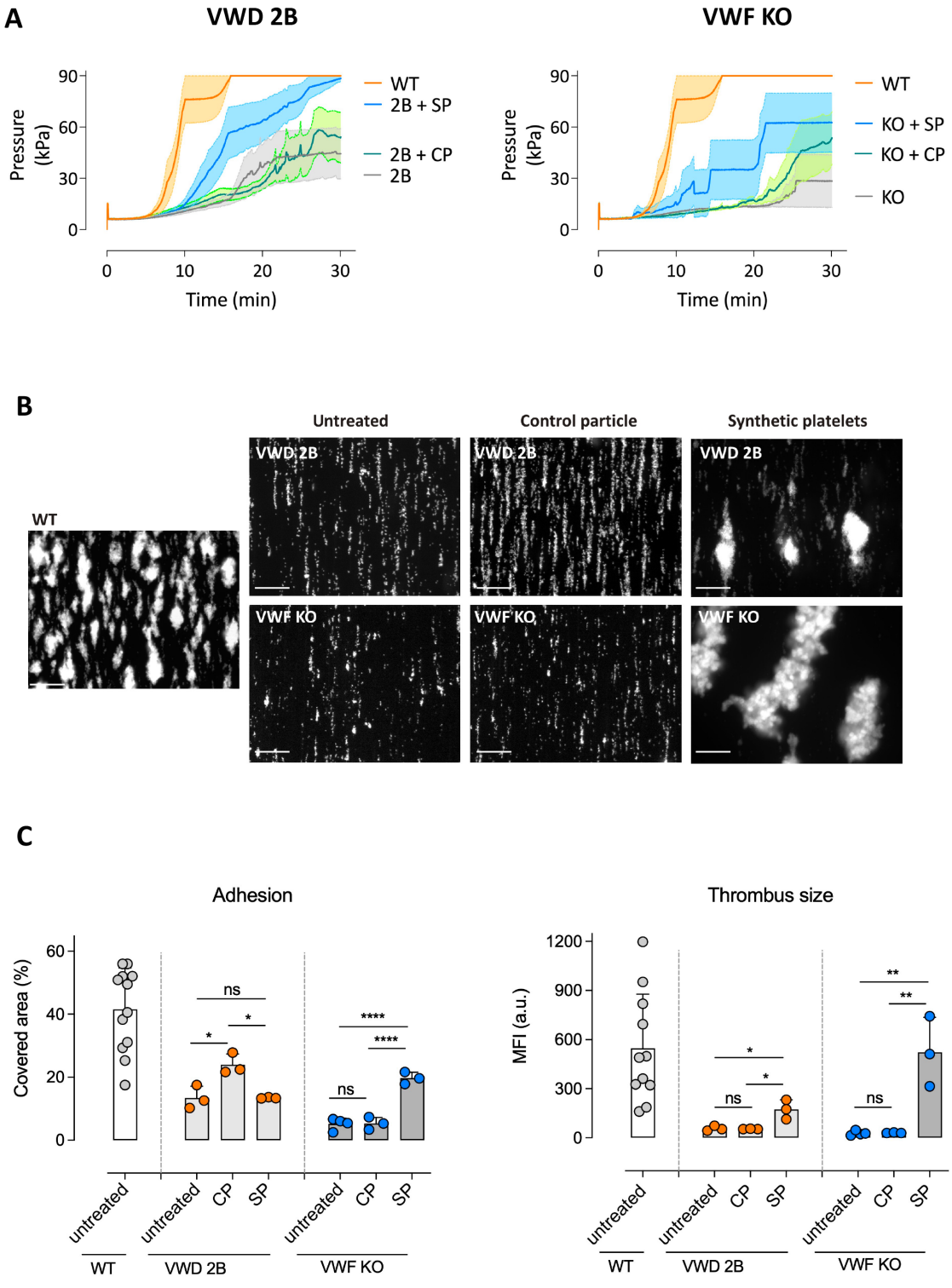
A
VWD 2B
VWF KO
Pressure (kPa)
Time (min)
WT
2B + SP
2B + CP
2B
KO + SP
KO + CP
KO
B
Untreated
Control particle
Synthetic platelets
WT
VWD 2B
VWF KO
C
Adhesion
Thrombus size
Covered area (%)
MFI (a.u.)
ns
untreated
CP
SP
WT
VWD 2B
VWF KO

Figure 3

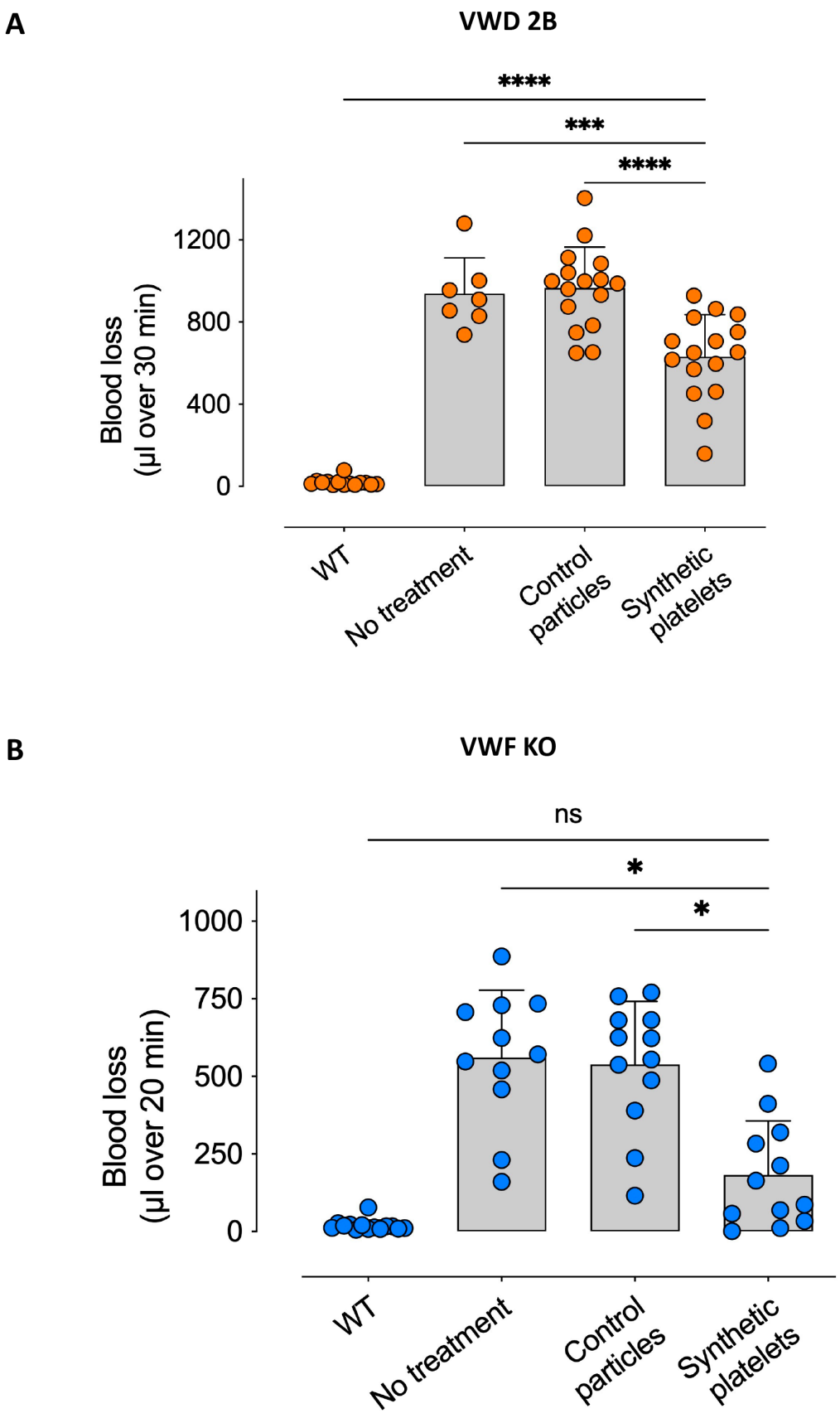
A
VWD 2B
****
***
****
Blood loss
(µl over 30 min)
1200
800
400
0
WT
No treatment
Control particles
Synthetic platelets
B
VWF KO
ns
*
*
Blood loss
(µl over 20 min)
1000
750
500
250
0
WT
No treatment
Control particles
Synthetic platelets

Figure 4

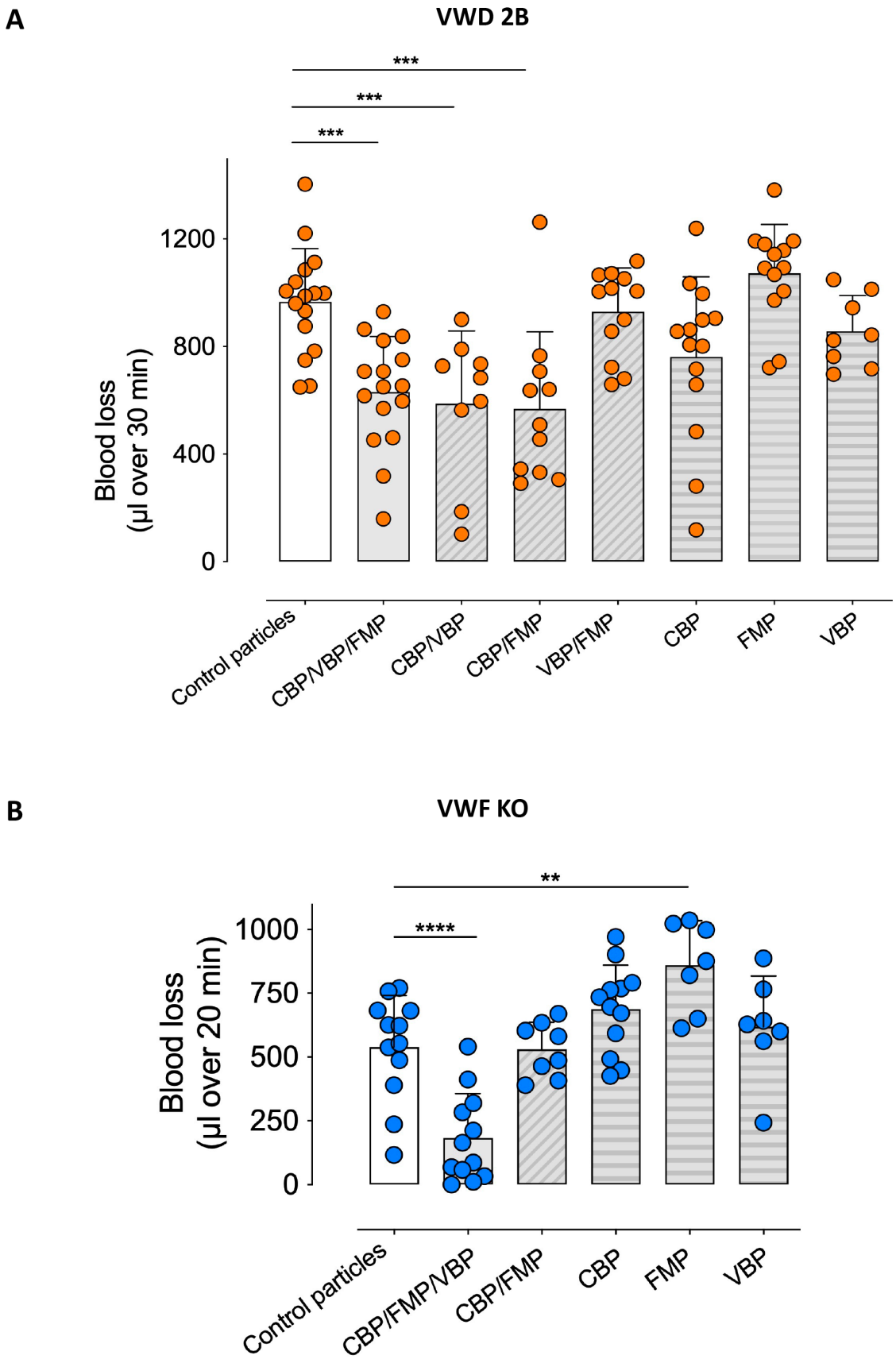
A
VWD 2B
***
***
***
Blood loss
(µl over 30 min)
1200
800
400
0
Control particles
CBP/VBP/FMP
CBP/VBP
CBP/FMP
VBP/FMP
CBP
FMP
VBP
B
VWF KO
**
****
Blood loss
(µl over 20 min)
1000
750
500
250
0
Control particles
CBP/FMP/VBP
CBP/FMP
CBP
FMP
VBP

Figure 5

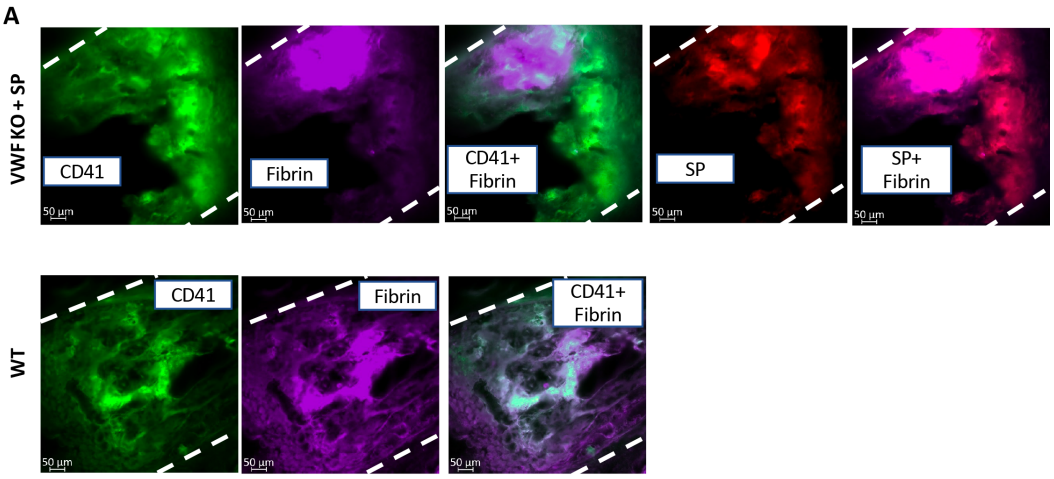
A
VWF KO + SP
CD41
Fibrin
CD41+ Fibrin
SP
SP+ Fibrin
WT
CD41
Fibrin
CD41+ Fibrin
50 µm

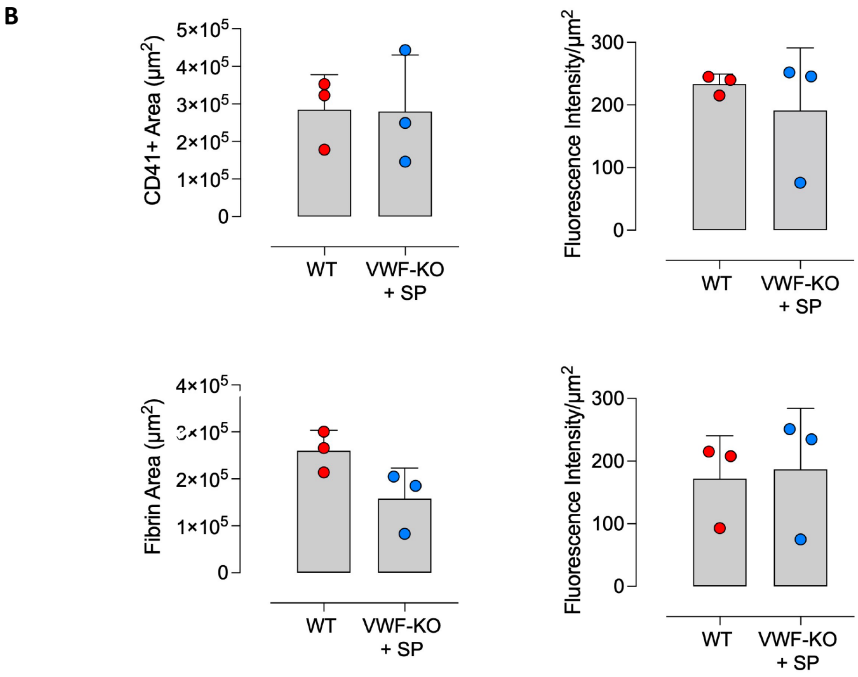
B
CD41+ Area (µm²)
5×10⁵
4×10⁵
3×10⁵
2×10⁵
1×10⁵
0
WT
VWF-KO + SP
Fluorescence Intensity/µm²
300
200
100
0
Fibrin Area (µm²)
Fibrin Area (µm²)
Fluorescence Intensity/µm²

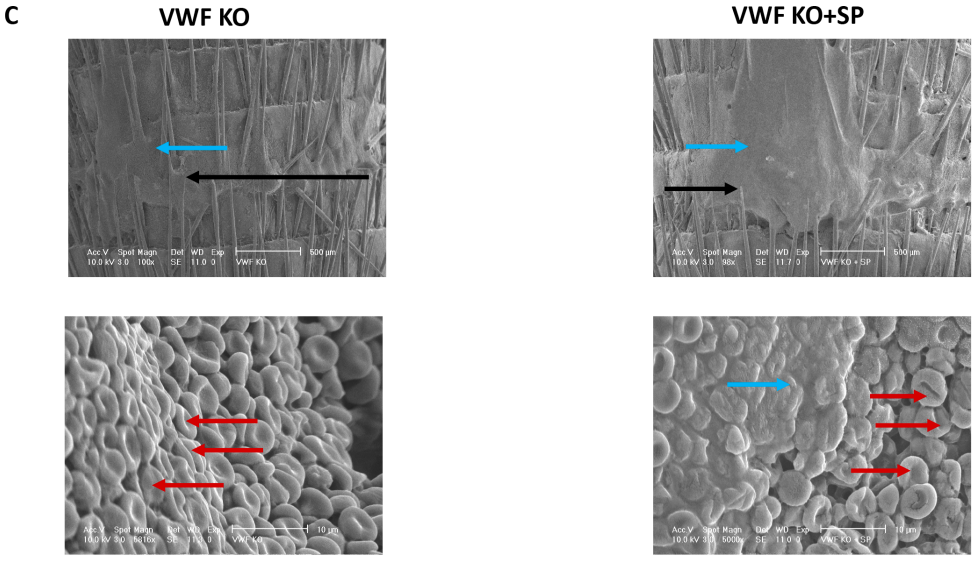
C
VWF KO
VWF KO+SP